Surface differential reflectivity for studying surface state optical transitions—a review

2004 J. Phys.: Condens. Matter 16 S4243

(http://iopscience.iop.org/0953-8984/16/39/001)

INSTITUTE OF PHYSICS PUBLISHING JOURNAL OF PHYSICS: CONDENSED MATTER

J. Phys.: Condens. Matter **16** (2004) S4243–S4258 PII: S0953-8984(04)78636-1

Surface differential reflectivity for studying surface state optical transitions—a review

A Cricenti

Istituto di Struttura della Materia, CNR, via Fosso del Cavaliere 100, 00133 Roma, Italy

E-mail: cricenti@ism.cnr.it

Received 30 March 2004
Published 17 September 2004
Online at stacks.iop.org/JPhysCM/16/S4243
doi:10.1088/0953-8984/16/39/001

Abstract

In this paper we present an overview of the method of surface differential reflectivity (SDR) for the study of semiconductor surfaces. We will describe the principles of the technique and the experimental apparatus together with some theoretical considerations concerning the connection of SDR with the microscopic properties of the surface. In particular, the analysis of SDR is done in the frame of a macroscopic three layers model in which the media involved (vacuum, surface and substrate) are assumed to have definite anisotropic dielectric functions. A few experimental results, indicative of the potential of the technique, will be shown.

1. Introduction

Semiconductor surfaces have been the subject of a great deal of theoretical and experimental research, concerning both their atomic and electronic properties [1]. A variety of experimental techniques and methods have been developed to investigate the electronic and vibrational properties as well as the structure of the surface. Realistic calculations of the two dimensional structure taking into account different reconstructions and surface imperfections are now available. This allows a comparison of theoretical models with experimental results, greatly advancing the knowledge of surface properties.

Optical methods have proved to be very useful in the study of surfaces [2–15]: however, in order to investigate the optical properties of surfaces one should consider that light penetrates the solid for a depth of α^{-1} (α being the absorption coefficient), a length much larger than the z-extension of the surface. It is possible to estimate that the surface contribution to the reflectivity of a semiconductor can be in the 10^{-2} range. The problem of discriminating bulk and surface effects is then of utmost importance, and the detection of such a small change of reflectivity requires a very accurate control of the stability of the optical system during the experiment.

In this frame surface differential reflectivity (SDR) [1] has proved to be very useful in the study of surfaces. SDR spectroscopy consists of measuring the reflectivity of a sample when the surface is clean and after its exposure to an external gas. In the following, for the sake of simplicity, we shall always refer to molecular oxygen as the contaminating gas, even though the discussion maintains its validity also for other gases. The results are given in terms of $\Delta R/R$ (also $\mathrm{D}R/R$ from now on), i.e., the relative variation of reflectivity between these two conditions:

$$\mathrm{D}R/R = (R_{\mathrm{clean}} - R_{\mathrm{ox}}(E))/R_{\mathrm{ox}}(E), \tag{1}$$

where R_{ox} is the saturation value of reflectivity after a prolonged oxygen exposure (E). Qualitatively, the reflectivity at a clean surface is larger than after oxidation, when surface states are removed. For photon energies lower than the semiconductor energy gap a $\mathrm{D}R/R$ spectrum has a straightforward physical meaning since it has been demonstrated that the structures observed in $\mathrm{D}R/R$ are proportional to the imaginary part of the surface dielectric function (SDF) [16, 17]. For photon energies larger than the gap, the interpretation of $\mathrm{D}R/R$ spectrum is not so simple, because of the absorption of the underlying bulk and the related structures in the real part of the surface dielectric constant together with the optical properties of the freshly formed oxide [18–20]. This calls for a more quantitative and deeper analysis to extract the dielectric properties of the surface layer from $\mathrm{D}R/R$ data.

It is then possible to say that the variation of sample reflectivity after oxygen adsorption is due to [21, 22]: (i) the disappearance of surface states; (ii) the variation of the Franz–Keldish (FK) effect in the space charge region; (iii) the optical properties of the growing oxide layer. It is possible to write:

$$\mathrm{D}R/R = (\mathrm{D}R/R)_{\mathrm{ss}} + (\mathrm{D}R/R)_{\mathrm{FK}} + (\mathrm{D}R/R)_{\mathrm{ox}}.$$

The $(\mathrm{D}R/R)_{\mathrm{ss}}$ contribution in the SDR spectra can help us to determine energy gaps between occupied and empty surface states, both unknown and known from other experiments. On the other hand, the strength of surface excitonic effects can be determined if some independent information about the relative position of the states involved in the optical transition is available [23], through angle resolved direct and inverse photoemission.

The $(\mathrm{D}R/R)_{\mathrm{FK}}$ term is related to the FK effect [24, 25] that consists of the variation of the optical properties of a crystal caused by an external electric field. Characteristic oscillatory structures appear in correspondence to bulk critical points [26]. This is indeed the basis of electroreflectance spectroscopy, in which a modulated external field applied normal to the surface gives rise to a reflectivity signal. In this way oscillatory features with maxima (or minima) corresponding to critical points of the bulk band structure are observed. In SDR experiments the change in band bending caused by the oxidation or by an external source, like a laser, determines a change of the built-in surface electric field and thus a variation of the FK contribution to reflectivity.

Since band bending is connected to the Fermi level position, a monitoring of the FK amplitudes allows an estimate of the Fermi level position as a function of oxygen exposure. Moreover, the possibility of measuring Fermi level movement as a function of oxygen exposure or metal evaporation [27–29] has the advantage that, in the case of metal islands on a semiconductor, the FK effect is induced only from the areas of the surface where the metal has adsorbed, i.e., those places where the local band bending has changed. The areas of the surface which are metal free give no contribution to the FK effect: in this way we get rid of work function inhomogeneity in non-uniform metal/semiconductor interfaces. In this context every kind of metal can be used on any semiconductor regardless of their work function. Another advantage, over other techniques, is the fact that the power is very small and does not give rise to the so-called surface photovoltage (SPV) effect. In fact, it has been shown

in the last few years that great care must be used for a good evaluation of Schottky barrier heights from photoemission data due to the presence of beam induced SPV [30]. Typical reflectivity variations due to the FK effect are of the order of 0.2% or less. These changes are usually smaller than the surface contribution to reflectivity. Nevertheless, they can be detected, especially in materials with high values of the electroreflectance coefficients as, for example, the III–V compounds.

The observation of the optical transitions sensitive to a surface contamination is also an useful tool for studying the oxidation process [29, 31–33]. This information is contained in the $(\mathrm{D}R/R)_{\mathrm{ox}}$ term and it may help us to determine the sticking coefficient and to find out which states are involved in the adsorption process of the molecules.

In order to relate reflectivity changes to surface physical properties, a detailed analysis based on the electromagnetic equations is necessary. The analysis of $\mathrm{D}R/R$ is done in the frame of a macroscopic three layers model in which the media involved (vacuum, surface (or oxide) and substrate) are assumed to have definite anisotropic dielectric function [34].

In this paper the SDR technique and its application to the study of the optical properties of clean semiconductor surfaces, are discussed in detail. A few experimental results, indicative of the potential of the technique, will be shown.

2. Experimental details

SDR spectroscopy involves measuring the reflectivity of a sample when the surface is clean and after an exposure (E) to an external gas [11, 12]. The experimental results are given in terms of $\mathrm{D}R/R(E)$, i.e., the relative variation of reflectivity between these two conditions:

$\mathrm{D}R/R(E) = [R_{\mathrm{clean}} - R_{\mathrm{ox}}(E)]/R_{\mathrm{ox}}(E)$, where $R_{\mathrm{ox}}(E)$ refers to the case of oxygen as the contaminating gas. The variation of sample reflectivity is due to: (i) the disappearance of surface states; (ii) the variation of the Franz–Keldish effect in the space charge region; (iii) the optical properties of the growing oxide layer.

A quantitative analysis of SDR spectra can be done in the frame of the macroscopic theory developed by Mclntyre and Aspnes [34], in which the surface is treated as an absorbing film of thickness d, much smaller than the light wavelength λ, on top of a semi-infinite solid. The media involved, including the surface, are assumed to have definite dielectric functions $\varepsilon_j = \varepsilon'_j - i\varepsilon''_j$, where $j = 1, 2, 3$ labels the three media (external, surface and substrate). For normal incidence and vacuum as external medium, one obtains

$$\mathrm{D}R/R = [R(d) - R(0)]/R(0) = (8\pi d/\lambda)\,\mathrm{Im}[(1-\varepsilon_2)/(1-\varepsilon_3)], \tag{2}$$

where $R(0)$ is the reflectivity when no absorbing film is present.

Despite its crudeness, this macroscopic model is known to give results in fair agreement with experiments. On the other hand, it can be demonstrated [35] that microscopic theories of surface reflectance [36, 37] yield substantially the same results (in the perturbative limit and for s-polarized light). Following such theories, the quantities entering in the macroscopic model are to be interpreted as appropriate spatial averages with respect to the surface normal.

Equation (2) has been obtained in the limit of very small d/λ: an alternative solution of the problem [38] can be found by means of the Abeles matrix method [39], that gives the same result as equation (2) in the same limit.

In order to apply equation (2) for the analysis of SDR data, the simplifying assumption $d_{\mathrm{ox}} = d$, d_{ox} being the thickness of the oxide monolayer, is made since both d and d_{ox} are of the order of a few ångströms. One easily obtains

$$\begin{aligned}\mathrm{D}R/R = {} & -8\pi d/\lambda[(1-\varepsilon'_{\mathrm{b}})(\varepsilon''_{\mathrm{s}} - \varepsilon''_{\mathrm{ox}})]/[(1-\varepsilon'_{\mathrm{b}})^2 + (\varepsilon''_{\mathrm{b}})^2] \\ & + \varepsilon''_{\mathrm{b}}(\varepsilon'_{\mathrm{s}} - \varepsilon'_{\mathrm{ox}})/[(1-\varepsilon'_{\mathrm{b}})^2 + (\varepsilon''_{\mathrm{b}})^2],\end{aligned} \tag{3}$$

where s (surface) and ox (oxide) refer to the second medium and b (bulk) to the substrate. The general case $d_{ox} \neq d$ is obtained by considering in equation (3) an effective dielectric function for the oxide, defined as

$$(\varepsilon_{ox})_{eff} = [(\varepsilon_{ox} + 1)d_{ox}/d - 1]$$

as can be easily seen by algebraic manipulation of equations (2) and (3).

In principle, optical transitions characteristic of the oxide layer cannot be ruled out, because of the presence of ε''_{ox} in equation (3). However, oxides are usually transparent in the considered spectral range: no oxygen induced transitions have been detected by other surface sensitive techniques (for example, electron energy loss) in our energy range. Therefore, in most of the cases, we can reasonably assume $\varepsilon''_{ox} = 0$ in equation (3).

We are thus left with the following expression:

$$\text{Error!} = d[A(\varepsilon''_s - \varepsilon''_{ox}) - B(\varepsilon'_s - \varepsilon'_{ox})], \tag{4}$$

where the dependence on the bulk properties is contained in the quantities

$$A = 8(\pi/\lambda)(\varepsilon'_b - 1)/[(1 - \varepsilon'_b)^2 + (\varepsilon''_b)^2] \tag{5}$$

and

$$B = 8(\pi/\lambda)\varepsilon''_b/[(1 - \varepsilon'_b)^2 + (\varepsilon''_b)^2]. \tag{6}$$

A knowledge of the bulk dielectric function is, therefore, necessary to extract the surface contribution. However, when the bulk substrate is not absorbing ($\varepsilon''_b = 0$), like for semiconductors below the gap, $B = 0$ and the measured change in reflectivity immediately yields $\varepsilon''_s d$. For photon energies above the gap, the second term in equation (4), contributing even when no surface states are present, cannot in principle be neglected. Such a term, however, is generally quite small for photon energies below 3.2 eV for Si, 2 eV for Ge, 2.8 eV for GaAs, and 3.5 eV for GaP. Figure 1 shows the coefficients A and B plotted versus photon energy for these four compounds.

When $B \neq 0$, the second contribution has to be included, and the DR/R spectrum is related to both the absorptive and dispersive parts of the surface dielectric function. It is also necessary to know ε'_{ox}, though a constant value of the order of unity can presumably be assumed, since the oxide layer is transparent for photon energies below 4 eV. Values ranging from 2 to 3, obtained from atomic polarizability data, are reported in literature.

In conclusion, the knowledge of DR/R over a sufficiently broad spectrum allows the determination of the complex dielectric function associated with the surface, through equations (4)–(6) and Kramers–Kronig (KK) relations (yielding an additional equation between ε'_s and ε''_s).

In fact, it is well known that the real and imaginary parts of the dielectric function are connected by the Kramers–Kronig (KK) dispersion relations:

$$\varepsilon'(\omega) = 1 + \frac{2}{\pi}\wp\int_0^\infty \frac{\omega'\varepsilon''(\omega')}{\omega'^2 - \omega^2}\,d\omega' \tag{7}$$

$$\varepsilon''(\omega) = \frac{2\omega}{\pi}\wp\int_0^\infty \frac{\varepsilon'(\omega') - 1}{\omega'^2 - \omega^2}\,d\omega', \tag{8}$$

where $\wp$ means the Cauchy principal part of the integral. KK relations are based uniquely on causality principle and linear response and have then general applicability.

Figure 2 shows the ultra-high vacuum (UHV) chamber together with the optical experimental set-up. After preparation by cleavage or sputtering and annealing, the surfaces are examined by means of the standard angle resolved valence band and core-level photoemission,

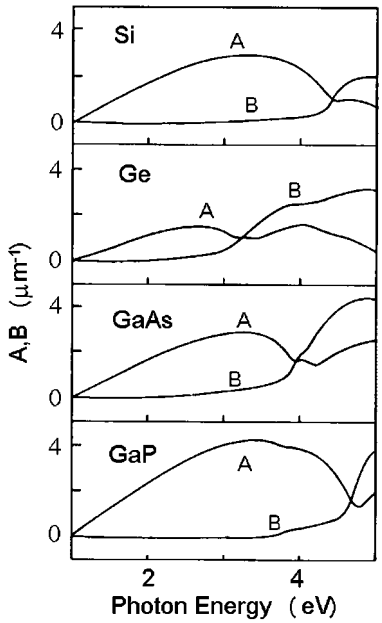

Figure 1. Energy dependence of the bulk coefficients A and B for Si, Ge, GaAs and GaP.

Auger and low-energy electron diffraction (LEED). This is an important step in order to be sure that the surface we are dealing with in the optical set-up is the one that we want to study.

In the optical apparatus the light emitted from a 150 W tungsten lamp is passed through a lens and is separated into two beams through a semi-transparent CaF_2 beam-splitter which directs 50% of the light at normal incidence to the sample. One beam (I) is focused through another lens on the surface into the UHV chamber through a CaF_2 window. The window is tilted 5° with respect to the sample surface, in order to spatially separate the reflections from the sample and from the window. The second beam (Io) is focused onto a dummy sample (usually of the same material under investigation or an aluminium mirror), which serves as the reference, in order to minimize spurious structures in the reflectivity spectrum. The reflected light from either the sample or the reference was dispersed in an EG&G PARC half-metre spectrometer with an optical multichannel analyser (OMA) mounted at the exit slit. The intensities of the two reflected beams are so measured by the OMA and the spectrum is stored in a personal computer through an IEEE 488 interface. The data stored are the values of the ratio between the reflectivity of the clean surface and the reflectivity of the dummy sample, normalizing with respect to the background signal through four computer controlled shutters. A 600 nm long wavelength pass filter is used to cut out laser light reflected off the sample and to get rid of higher orders of the monochromator. The emission lines from an Hg lamp were used to calibrate the wavelength response of the spectrometer to within 1 meV. The DR/R experimental accuracy was better than 2×10^{-4} over several hours.

3. Experimental results

In order to illustrate the accuracy and reliability of the SDR method and the procedure for obtaining the surface optical functions, we briefly discuss the experimental results for Si(111)2×1, Si(100)–Sb, InP(110) and CdTe(110).

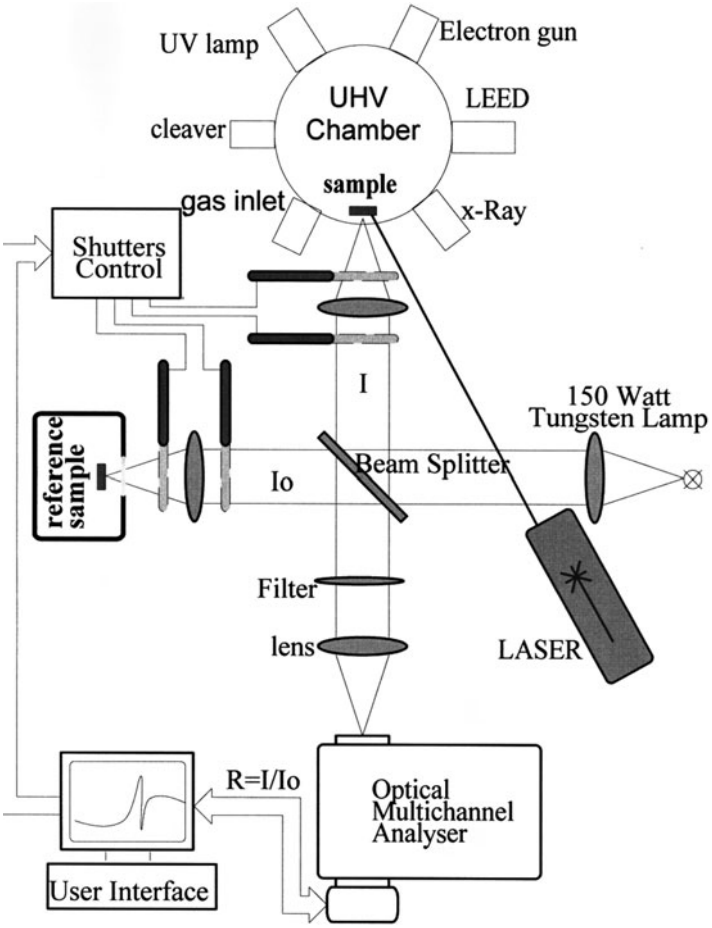

Figure 2. The optical set-up with the UHV chamber.

3.1. SDR as a test for surface structure: Si(111)2 × 1

Upon cleavage at room temperature, the Si(111) surface reconstructs to a metastable 2 × 1 structure, with two surface atoms per surface unit cell. The exact nature of this reconstruction was an open question. Early models for the 2 × 1 reconstruction were centred around a buckling mechanism [40] which involves the raising and lowering of adjacent rows of surface atoms from their ideal bulk positions. An alternative model, proposed by Pandey [41, 42], involved Π-bonded chains along the (110) direction of the Si(111)2 × 1 surface with a major rearrangement of the atoms in the top few atomic layers. Although the buckling and chain models predicted a similar optical gap, the expected polarization dependence of the optical absorption was quite different. For the chain model, the absorption was maximal for light polarized parallel to the chains, whereas for the buckling model the maximum absorption occurred for light polarized perpendicular to the rows of atoms.

Figure 3 shows the SDR spectrum of an Si(111)2 × 1 surface obtained at room temperature with unpolarized light in the 0.3–0.7 eV photon-energy range [17]. The surface was obtained by cleaving a silicon sample in ultra-high vacuum condition and by taking $\mathrm{D}R/R$ on the clean surface and after oxidation. This result was the first evidence of the existence of

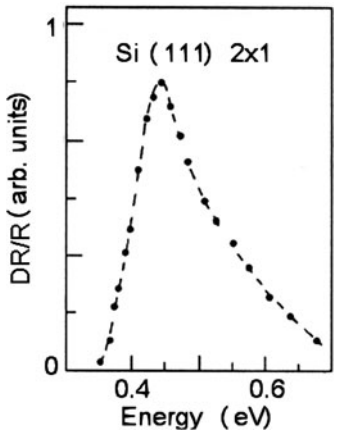

Figure 3. Surface differential reflectivity spectrum of Si(111)2 × 1 at room temperature in the 0.3–0.7 eV photon range.

a gap in the dangling-bond band split by the 2 × 1 reconstruction. By using polarized light the only contribution in the SDR spectra was with the light electric vector parallel to the [110] direction [43, 44]. Such measurement, together with a theoretical analysis [45] of the polarization dependence of surface reflectivity in Si(111)2 × 1, is among the first experimental evidences of the validity of Pandey's model for the 2 × 1 reconstruction. In fact, as successively observed by scanning tunnelling microscopy (STM) [46], the surface is strongly anisotropic with the principal axes of the surface dielectric tensor along the directions of the 2 × 1 reconstruction.

For photon energies below the bulk gap the SDR spectrum immediately gives the imaginary part of the surface dielectric function. In fact the B term entering equation (4) is zero in the whole range where surface transitions occur (see figure 1).

The great anisotropy of the optical transitions suggested that we should perform an experiment by reflection anisotropy spectroscopy (RAS) [47]. This experiment in the near infrared, IR-RAS, does not require an oxidation of the surface and the spectrum is practically the same as that obtained by SDR shown in figure 3, as should be expected, since the surface is approximately absorbing only with the light electric vector parallel to the [110] direction over the entire energy range.

3.2. Metal overlayer: the case of Si(100)*Sb*-1 × 1 *and* 2 × 1

The SDR spectra for the Si(100)–Sb surfaces [48, 49] were recorded from a surface obtained by evaporating 4 ML of Sb onto a clean Si(100)2 × 1 surface kept at room temperature followed by annealing at temperatures ranging from 350 to 550 °C. The resulting LEED pattern was a clear 1 × 1 (350 °C) and a two-domain 2 × 1 spots (450 °C).

With our apparatus a single spectrum (between 1.3 and 3.0 eV) was recorded in approximately 30 s so that the optical peak could be followed during the annealing process. The results are given in terms of DR/R, i.e., the change in sample reflectivity during annealing: D$R/R = (R_{an} - R_0)/R_0$. R_{an} is the annealed surface while R_0 is the surface after the Sb evaporation and with the sample that has just reached 350 °C. At this temperature all but one monolayer (ML) of Sb desorbs so that we get rid of the contribution to reflectivity of the Sb atoms exceeding 1 ML. As we have seen, for photon energies below 3.2 eV, DR/R gives the

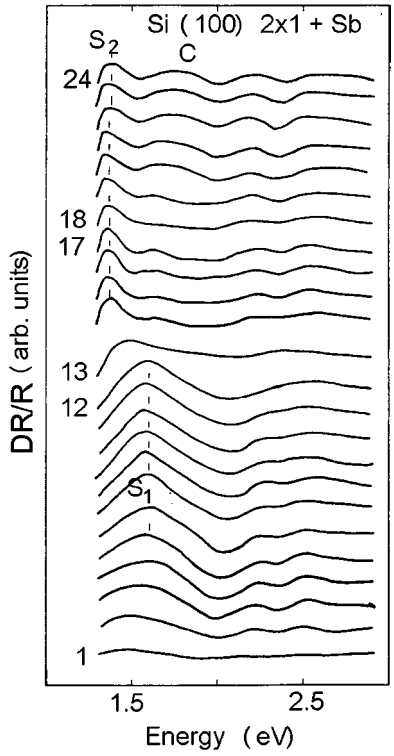

Figure 4. Sb onto Si(100)2 × 1: evolution of surface differential reflectivity spectra in the 1.3–3.0 eV photon range at different temperatures as a function of time.

imaginary part of the surface dielectric function directly. Thus within our experimental range (1.3–3.0 eV), DR/R gives only transitions between surface states in the antimony covered surfaces.

Figure 4 shows the DR/R variation as a function of the annealing time and sample temperature. With the sample at 350 °C (1 × 1-Sb surface) a prominent peak (S_1) is observed to develop at 1.6 eV (see spectra 1–12). Upon annealing the sample at 450 °C (Sb-2 × 1 phase) the peak S_1 is suppressed and a new structure (S_2) develops around 1.4 eV (see spectra 13–17). Both S_1 and S_2 peaks give the minimum energy gap for surface state transition. Upon further annealing at 550 °C the Sb atoms start to desorb so that part of the surface returns to being clean: this is clearly evidenced in the SDR spectra 18–24 by a decreasing of the Sb-induced peak at 1.4 eV and by the growth of the clean Si(100)2 × 1 peak around 1.7 eV.

3.3. SDR to observe changes in Fermi level pinning: CdTe(110)

Schottky barrier heights have been usually measured with photoemission from the valence band and from core levels [50]. However, the work function of a semiconductor may be changed by the absorption of light [30, 51, 52]. The difference of the work function measured under illumination and in the dark is the so-called surface photovoltage. In this context, it has been shown in the last few years that great care must be used for a good evaluation of Schottky barrier heights from photoemission data due to the presence of beam induced SPV [30]. In fact, photoemission results on the Ag/GaP(110) system needed to be corrected for the induced

photovoltage by measuring the contact potential difference between the sample illuminated by the synchrotron beam and the sample obscured.

Also a Kelvin probe can be used to evaluate Schottky barrier heights through contact potential difference (CPD) measurements [53]: however, in this case the experiments must also be restricted to study barrier heights where the metal and the semiconductor have similar work function. In fact, in the case of metal islands on a semiconductor, we can, reasonably, assume that a Kelvin probe measures some kind of averaged work function. This is due to the large electrode area (a few millimetres) that probe simultaneously the metal islands and the semiconductor free regions, unless one uses a microkelvin probe with a very thin electrode (a few nanometres), that might probe different areas on the same sample. In the general case this averaged work function is neither the semiconductor one, nor the metal one, and will depend on coverage and island extension.

As we have already pointed out, the Franz–Keldish effect also gives the possibility of measuring Fermi level movement as a function of oxygen exposure or metal evaporation. The advantage of such a method over the Kelvin probe is that, in the case of metal islands on a semiconductor, the FK effect is induced only from the areas of the surface where the metal has adsorbed, i.e., those places where the local band bending has changed. The areas of the surface which are metal free give no contribution to the FK effect: in this way we get rid of work function inhomogeneity in non-uniform metal/semiconductor interfaces. In this context every kind of metal can be used on any semiconductor regardless of their work function. Moreover, in comparison with photoemission, the energy resolution by using the FK method is much higher (a few meV against several tens of meV). Using the FK effect no absolute value of band bending can be directly measured, but differences and variations in band bending may be determined with excellent precision and without disturbing the surface by the measurement itself.

Laser induced band bending variations on ultra-high vacuum cleaved CdTe(110)1×1 surfaces [54–56] kept at room temperature were observed through the FK effect by focusing an Ar laser beam (5500 A Ion Laser Technology, 457–514.5 nm) to a 5×5 mm^2 spot on the sample surface. The incidence angle of the laser beam on the sample was 30°. The SDR spectrum is the difference of the reflectivity of the sample with and without the laser beam.

$$\mathrm{SDR} = \frac{\Delta R}{R_0} = \frac{R_1 - R_0}{R_0}, \tag{9}$$

where R_1 and R_0 are the reflectivity of the samples measured with the laser on and off, respectively.

Figure 5 shows a complete set of $\Delta R/R$ spectra for laser power between 100 and 500 mW. The shape of the FK oscillation does not change with laser power while the oscillation amplitude increases linearly up to a laser power of 400 mW with a faster increase observed for higher laser power. The linear trend is in accordance with the calculation of electric field induced changes in $\Delta R/R$ at a parabolic point edge [57]. The maximum FK amplitude (2.5%) is observed for a laser power $P = 500$ mW and corresponds to a 0.2 eV shift observed with angle resolved photoemission (ARPES). The FK oscillation amplitude of figure 5, then, represents the movement of the FL at the surface with a maximum shift of 0.2 eV towards bulk mid-gap.

After turning off the laser the FK amplitude tends to decrease quite slowly: the experimental points are well described by an exponential decay with a time constant of 1300 s. Such a long discharging time indicates the existence of traps, in the band bending region near the surface, for the electron–hole pairs generated by the laser light.

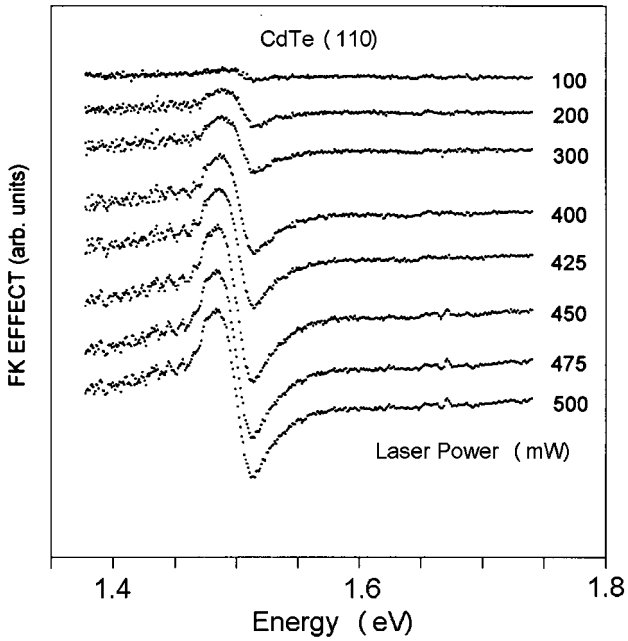

Figure 5. Reflectivity variation brought about by laser irradiation for a cleaved CdTe(110) surface with laser power between 100 and 500 mW.

3.4. A mixed case: InP(110)

InP n-type samples were cleaved in a UHV environment with the double wedge technique obtaining reproducible flat mirror-like surfaces. The reflectivity variation brought about by the oxidation of a clean cleaved InP(110) surface [21, 22, 29, 59–61] was measured as a function of the photon energy in the range 2.0–4.0 eV. Figure 6 shows DR/R for two different exposures (2×10^3 (curve b) and 2×10^6 L O_2 (curve a)). The lower exposure curve clearly shows characteristic FK oscillations around 3.15 eV, corresponding to a bulk saddle point of type M_1 [58]. The figure shows that the FK oscillations almost disappear at the highest exposures, when presumably the band bending returns to its initial value.

As we have seen, there are mainly three terms in an SDR spectrum: $DR/R = (DR/R)_{ss} + (DR/R)_{FK} + (DR/R)_{ox}$. In the case of InP(110) they all contribute to the optical spectrum, and in order to discriminate among the different contributions we have measured the reflectivity variation as a function of oxygen exposure at three different photon energies: 3.14 eV (corresponding to the minimum of FK first oscillation) [58], 3.22 eV (corresponding to the maximum of FK first oscillation) [58], and 3.58 eV (a region near the threshold of In_2O_3 absorption [61]). The choice of the photon energies for monitoring the FK amplitude depends on the doping of the sample [58].

Below the threshold for oxide absorption it is possible to write approximately

$$DR/R = (DR/R)_{ss} + (DR/R)_{FK}.$$

The value

$$(DR/R)_{ss} = (1/2)[(DR/R)_2 + (DR/R)_1]$$

(where 1 and 2 refer to 3.14 and 3.22 eV, respectively) gives the surface states contribution directly in the intermediate point where the FK contribution is zero. On the other hand the

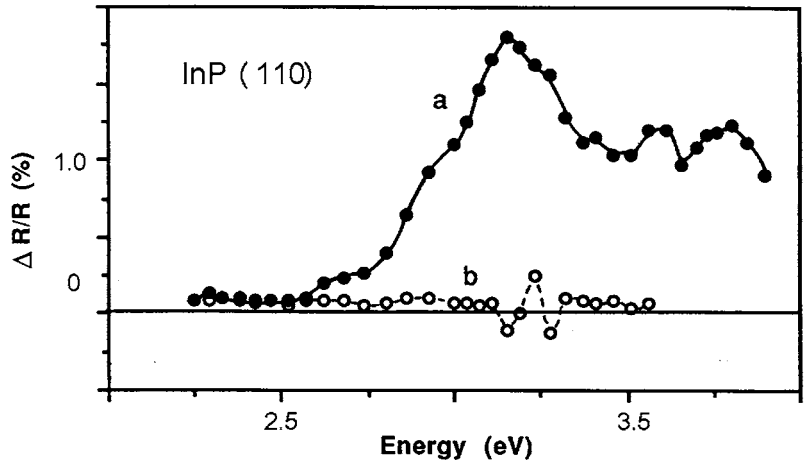

Figure 6. Differential reflectivity for cleaved InP(110) surfaces. Curve a (solid line, full circles) refers to a complete oxidation (2×10^6 L); curve b (dashed line, open circles) refers to the initial stage of oxidation (2×10^3 L).

amplitude of the FK oscillation can be obtained from

$$(\mathrm{D}R/R)_{\mathrm{FK}} = (\mathrm{D}R/R)_2 - (\mathrm{D}R/R)_1$$

and from the values of $(\mathrm{D}R/R)_{\mathrm{ss}}$ at the energies 3.22 and 3.14 eV that can be obtained by interpolation between the values of $\mathrm{D}R/R$ at energies before and after FK oscillations.

The dependence of $(\mathrm{D}R/R)_{\mathrm{ss}}$ and $(\mathrm{D}R/R)_{\mathrm{FK}}$ as a function of exposure is reported in figures 7(a) and (b), respectively. The comparison of the two figures, particularly the difference of threshold and the different behaviour at high values of exposure, shows clearly that the states that control the position of the Fermi level at the surface are not (or are not uniquely) the intrinsic surface states. The conclusion is also supported by curve b of figure 6, that shows remarkable FK oscillations, i.e., a strong variation of band bending occurring in the absence of appreciable disappearance of surface states.

The general behaviour of band bending, that goes through a maximum and reverts towards the value of the clean surface for large exposures, agrees with the photoemission experiments. The inversion of the Fermi level movement can be due to native shallow donor defects that compensate the charge of the acceptor states, responsible for the initial increase of band bending [62]. At higher coverages (10^5 L) the acceptor states are completely compensated and the Fermi level reaches a pinning position evidenced by the plateau of figure 7(b). In this range oxygen molecules are chemisorbed as phosphorous oxides like P_2O_3, P_2O_5, $InPO_4$ [63, 64]. At still higher exposures, In_2O_3 is formed, causing a further decrease of band bending associated with its intrinsic donor character. While phosphorous oxides are transparent in our energy range, In_2O_3 is strongly absorbing above 3.5 eV [61]. Because of the definition of $\mathrm{D}R/R$ in equation (1), the presence of an absorption due to the oxide (In_2O_3) should give a negative contribution. This is clearly seen in the curve of figure 7(c) that reports $\mathrm{D}R/R$ at 3.58 eV as a function of exposure. The curve, in fact, presents a strong decrease in a region (above 2×10^5 L) where the surface states have already disappeared (see figure 7(a)). An analysis similar to that reported for the FK oscillations is somewhat difficult since the spectrum of the oxide is unknown. The formation of other oxides (P_2O_3, P_2O_5, $InPO_4$) has to be excluded since they are absorbing at energies larger than 4.5 eV [65].

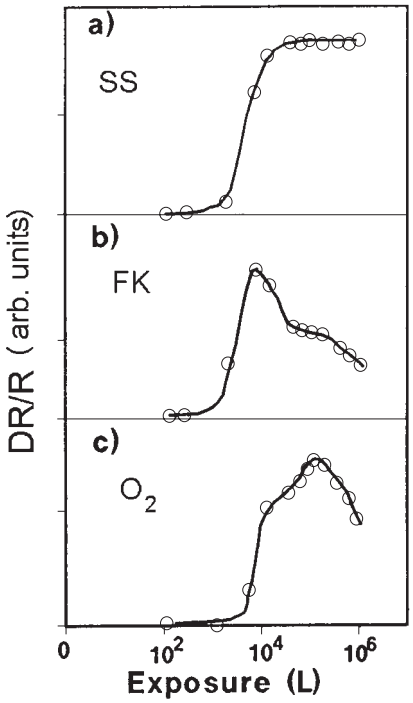

Figure 7. Surface states contribution $(\mathrm{D}R/R)_{\mathrm{ss}}$ (a), Franz–Keldish contribution $(\mathrm{D}R/R)_{\mathrm{FK}}$ (b) and oxide contribution at 3.58 eV (c) versus oxygen exposure for cleaved InP(110) surfaces.

3.5. The use of polarized light and the evaluation of the exciton contribution

SDR spectra can help us to determine energy gaps between occupied and empty states, both unknown and known from other experiments. On the other hand, the strength of surface excitonic effects can be determined if some independent information about the relative position of the states involved in the optical transition is available.

Undoped, p-type CdTe crystals were cleaved along the [110] direction by means of two wedges of different angle (30° and 60°) in a UHV preparation chamber attached to the main chamber [66–69]. This procedure gave us mirror-like surfaces of a 1×1 structure, as checked by LEED.

Figure 8 shows the energy dependence of the computed $\varepsilon_{\mathrm{s}}''$ for a light electric vector along the $[1\bar{1}0]$ (dashed curve) and [001] (full curve) directions, respectively. In this case $\frac{\Delta R}{R}$ and $\varepsilon_{\mathrm{s}}''$ are remarkably different because of the high value of the B term, particularly above 3.0 eV. This shows the importance of the method outlined above to analyse the optical data before comparing with experimentally derived or calculated surface state transitions. In the imaginary part of the dielectric function, the structure at 2.7 eV shows a marked dependence upon light polarization, being stronger for the light electric vector along the [001] direction. A shoulder around 3.3 eV is present for both light polarizations. The main peak at 3.7 eV is slightly reduced upon changing the light polarization. By comparing with ARPES and K-resolved inverse photoemission (KRIPES) band mapping we can assign the optical transition at 2.7 eV at the Γ point in the surface Brillouin zone, the one at 3.3 eV at Γ and X, and the one at 3.7 eV at X and X′. This fact of having several points in the SBZ contributing simultaneously in the SDR peaks is the reason for having such an isotropic behaviour in the polarization dependence

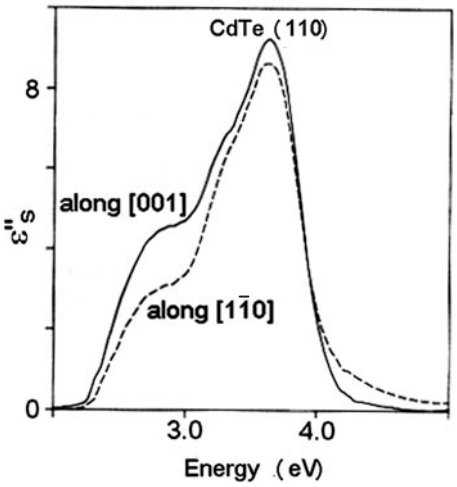

Figure 8. Computed ε''_s for a cleaved CdTe(110) surface. The light electric vector is polarized along the [1$\bar{1}$0] (dashed curve) and [001] (full curve) directions.

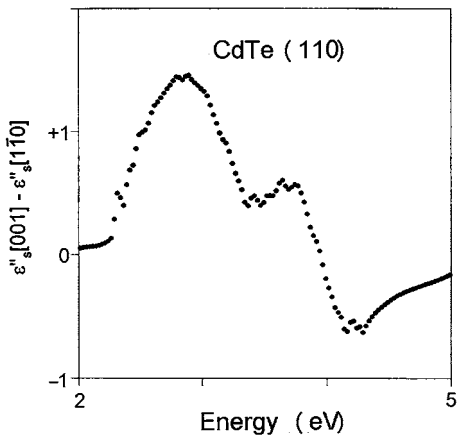

Figure 9. Difference between ε''_s for CdTe(110) computed along the [001] and along the [1$\bar{1}$0] directions.

of the surface dielectric function. Furthermore, these values correspond well to the energy gaps between occupied and empty surface states deduced from results of ARUPS [70] and KRIPES [71] experiments: this comparison of the energy of the optical excitations with the width of the gaps between the states observed by ARUPS and KRIPES shows that the surface excitonic binding energy in CdTe(110) surfaces is markedly smaller than that measured for Si(111)2 × 1 [72] or GaP(110) [23].

3.6. Comparison with RAS

SDR can be applied both to isotropic and to anisotropic surfaces, in the last case with polarized light. In order to better visualize the anisotropies in the CdTe(110) shown before in ε''_s we have plotted in figure 9 the difference between the two ε''_s. The anisotropy reaches its maximum at 2.8 eV for light polarized along the [001] direction; a second relative maximum is at 3.7 eV for the same polarization while a minimum (maximum for the other polarization) is present at 4.2 eV.

This anisotropy is the expected result in the case of a reflectance anisotropy spectroscopy experiment: in fact, in anisotropic surfaces, the RAS technique can be conveniently used. It does not require oxidation of the surface but it is limited, however, to the detection of the anisotropic part of the optical response.

In RAS the relative change of reflectivity is defined as

$$\Delta R/R = 2(R_x - R_y)/(R_x + R_y), \tag{10}$$

where R_x and R_y are the (near normal) reflection amplitudes for light polarized along two perpendicular directions x and y on the surface. RAS can be made very sensitive to small anisotropies, by using the technique of in-phase detection. The RAS signal given by (10) can be written, in the Aspnes and McIntyre formalism, as

$$S(\omega) = 2\frac{R_x(d) - R_y(d)}{R_x(d) + R_y(d)} \simeq 2\frac{R_x(d) - R_y(d)}{R_x(0) + R_y(0)}. \tag{11}$$

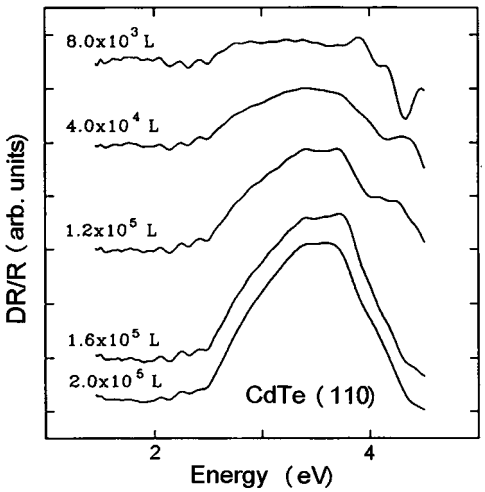

Figure 10. Evolution of the SDR spectra of a CdTe(110)1 × 1 in the 1.4–4.5 eV energy range as a function of oxygen exposure.

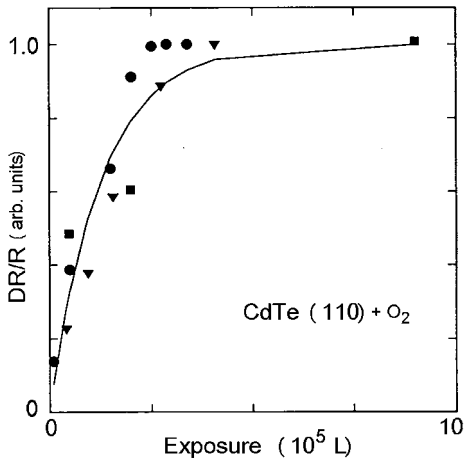

Figure 11. Intensity of the main spectral feature observed at 3.5 eV plotted as a function of oxygen exposure. The different symbols (circles, squares, and triangles) correspond to values measured for different cleavages and oxidation processes.

Since for an isotropic substrate $R_x(0) = R_y(0)$, we can write

$$S(\omega) = \left(\frac{\Delta R}{R}\right)_x - \left(\frac{\Delta R}{R}\right)_y = Ad(\varepsilon_x'' - \varepsilon_y'') - Bd(\varepsilon_x' - \varepsilon_y'), \tag{12}$$

which gives the RAS signal in terms of the anisotropic surface dielectric functions $\hat{\varepsilon}_x$ and $\hat{\varepsilon}_y$.

3.7. Oxidation of the surface

The observation of the optical transitions sensitive to a surface contamination is also a useful tool for studying the oxidation process. It may help us to determine the sticking coefficient and to find out which states are involved in the adsorption process. In fact, the basic argument for the connection of SDR spectra with the surface electronic structure is their sensitivity to oxidation of the sample. The strength of the change in surface reflectivity increases with growing exposure to the gas. Figure 10 shows the evolution of the SDR spectra for CdTe(110) surfaces [66] as a function of the exposures calculated as a product of the total pressure in the chamber and the period of gas adsorption on the surface.

Oxidation was obtained by introducing oxygen into the chamber up to a pressure of 1×10^{-5} Torr in about 1 min. Then the spectra were recorded during the further slow (about 2 h) increase of the amount of oxygen up to 5–8 $\times$ 10^{-5} Torr. The ion gauge was still on. Molecular oxygen, not excited by the ion gauge filament, did not cause any marked changes in the SDR spectra. Such an observation is consistent with the results of the previous studies of oxidation of II–VI compounds [73].

The partial pressures analysis has shown that some amount of carbon oxide was present in the chamber together with oxygen. It was produced by the hot filament of the ion gauge. From Auger spectroscopy measurements both oxygen and carbon were detected on the surface after the contamination process. The amount of carbon revealed on the surface was dependent on the course of the process. A faster increase of the oxygen pressure reduced the number of

carbon oxide molecules absorbed. However, this did not influence markedly the shape of the SDR spectra.

The growth of the main spectral feature at 3.5 eV was plotted as a function of the exposure in figure 11. The values are normalized to the strength of the saturated changes. The different symbols (circles, squares and triangles) correspond to results obtained for different cleavages and oxidation processes. This set of data enabled us to estimate the value for the sticking coefficient (k) in the initial stage of adsorption. We described the dependence of $\Delta R/R$ on the exposure (E) with the formula (according to the Langmuir model of adsorption [74]):

$$\Delta R/R(E) = 1 - \mathrm{e}^{-kE}. \tag{13}$$

The best fit to the experimental result was achieved for $k = 10^{-5}\ \mathrm{L}^{-1}$. This value is similar to that found for III–V crystals, but not for excited molecular oxygen [11]. CdTe resists much more strongly against the ambient atmosphere than the previously studied compounds.

4. Conclusions

The method of surface differential reflectivity (SDR) for the study of semiconductor surfaces has been described with particular emphasis given to polarization and band bending studies.

References

[1] Luth H 1995 *Surfaces and Interfaces of Solid Materials* (Berlin: Springer)
[2] Chiarotti G 1994 *Surf. Sci.* **299/300** 541 and references therein
[3] Chiaradia P and Del Sole R 1999 *Surf. Rev. Lett.* **6** 517
[4] McGilp J F 1989 *J. Phys.: Condens. Matter* **1** SB85
[5] Aspnes D E 1985 *J. Vac. Sci. Technol.* B **3** 1498
[6] Berkovits V L *et al* 1985 *JETP Lett.* **41** 551
[7] Schmidt V G *et al* 2001 *Phys. Status Solidi* a **188** 1401
[8] Kamija I *et al* 1992 *Phys. Rev.* B **46** 24
[9] Martin D S and Weightman P 2002 *Surf. Interface Anal.* **31** 915 and references therein
[10] Olmstead M A 1986 *Surf. Sci. Rep.* **6** 159
[11] Selci S, Ciccacci F, Chiarotti G, Chiaradia P and Cricenti A 1987 *J. Vac. Sci. Technol.* A **5** 327
[12] Cricenti A, Selci S, Ciccacci F, Felici A C, Goletti C, Yong Z and Chiarotti G 1988 *Phys. Scr.* **38** 199
[13] Cricenti A (ed) 2001 *Epioptics 2000: Proc. 19th Course of the Int. School of Solid State Physics* (Singapore: World Scientific)
[14] Cricenti A (ed) 2004 *Epioptics-7: Proc. 24th Course of the Int. School of Solid State Physics* (Singapore: World Scientific)
[15] McGilp J F 1995 *Prog. Surf. Sci.* **49** 1
[16] Chiarotti G, Del Signore G and Nannarone S 1968 *Phys. Rev. Lett.* **21** 1170
[17] Chiarotti G, Nannarone S, Pastore R and Chiaradia P 1971 *Phys. Rev.* **134** 3398
[18] Nannarone S, Chiaradia P, Ciccacci F, Merneo R, Sassaroli P, Selci S and Chiarotti G 1980 *Solid State Commun.* **33** 593
[19] Wierenga E, van Silfhout A and Sparnay M J 1979 *Surf. Sci.* **87** 43
[20] Chiaradia P, Chiarotti G, Ciccacci F, Memeo R, Nannarone S, Sassaroli P and Selci S 1980 *Surf. Sci.* **99** 70
[21] Selci S, Cricenti A, Felici A C, Ferrari L, Goletti C and Chiarotti G 1991 *Phys. Rev.* B **43** 6757
[22] Cricenti A, Selci S, Felici A C, Ferrari L, Gavrilovich A, Goletti C and Chiarotti G 1991 *J. Vac. Sci. Technol.* A **9** 1026
[23] Riesterer T, Perfetti P, Tschudy M and Reihl B 1987 *Surf. Sci.* **189/190** 795
[24] Franz W 1958 *Z. Naturf.* a **13** 484
[25] Keldish L V 1958 *Sov. Phys.—JETP* **7** 788
[26] Seraphin O 1966 *J. Appl. Phys.* **37** 721
[27] Ciccacci F, Selci S, Chiarotti G, Chiaradia P and Cricenti A 1986 *Surf. Sci.* **168** 28
[28] Gaskill D K, Bottka N and Sillmon R S 1988 *J. Vac. Sci. Technol.* B **6** 1497
[29] Cricenti A, Selci S, Felici A C, Goletti C and Chiarotti G 1989 *Surf. Sci.* **211** 552

[30] Alonso M, Cimino R and Horn K 1990 *Phys. Rev. Lett.* **64** 1947
[31] Chiaradia P and Nannarone S 1976 *Surf. Sci.* **54** 547
[32] Wierenga P E, Sparnay M J and Van Silfhout A 1980 *Surf. Sci.* **99** 59
[33] Selci S, Chiaradia P, Ciccacci F, Cricenti A, Sparvieri N and Chiarotti G 1985 *Phys. Rev.* B **31** 4096
[34] Mclntyre D E and Aspnes D E 1971 *Surf. Sci.* **24** 417
[35] Del Sole R 1981 *Solid State Commun.* **37** 537
[36] Nakayarna M 1974 *J. Phys. Soc. Japan* **39** 265
[37] Bagchi A, Barrera R C and Rajagopal A K 1979 *Phys. Rev.* B **20** 4824
[38] Nannarone S and Selci S 1983 *Phys. Rev.* B **10** 5930
[39] Born M and Wolf E 1965 *Principles of Optics* (New York: Pergamon)
[40] Haneman D 1961 *Phys. Rev.* **121** 1093
[41] Pandey K C 1981 *Phys. Rev. Lett.* **47** 1913
[42] Pandey K C 1982 *Phys. Rev. Lett.* **48** 1032
[43] Chiaradia P, Cricenti A, Selci S and Chiarotti G 1984 *Phys. Rev. Lett.* **52** 1145
[44] Ciccacci F, Selci S, Chiarotti G and Chiaradia P 1986 *Phys. Rev. Lett.* **56** 2411
[45] Del Sole R and Selloni A 1984 *Solid State Commun.* **50** 825
[46] Feenstra R M, Thompson W A and Fein A P 1986 *Phys. Rev. Lett.* **56** 608
[47] Goletti C, Bussetti G, Arciprete F, Chiaradia P and Chiarotti G 2002 *Phys. Rev.* B **66** 153307
[48] Cricenti A, Selci S, Felici A C, Ferrari L and Chiarotti G 1993 *Solid State Commun.* **86** 667
[49] Cricenti A, Selci S, Felici A C, Ferrari L, Contini G and Chiarotti G 1993 *Phys. Rev.* B **47** 15745
[50] See for example: Chang S, Vitomirov I M, Brillson L J, Rioux D F, Kirchner P D, Pettit G D, Woodal J M and Hecth M H 1990 *Phys. Rev.* B **41** 12299
[51] Demuth E, Thompson W J, DiNardo N J and Imbihl R 1986 *Phys. Rev. Lett.* **56** 1408
[52] John P, Miller T, Hsieh T C, Shapiro A P, Wachs A L and Chiang T C 1986 *Phys. Rev.* B **34** 6704
[53] Koenders L, Ullrich H, Bartels F and Monch W 1985 *J. Vac. Sci. Technol.* B **3** 1107
[54] Cricenti A, Ferrari L, Orlowski B A and Kowalski B J 1995 *Vacuum* **46** 485
[55] Cricenti A and Orlowski B A 1995 *Phys. Rev.* B **51** 2322
[56] Cricenti A, Orlowski B A and Ferrari L 1995 *Surf. Sci.* **331** 1361
[57] Seraphin B O and Bottka N 1966 *Phys. Rev.* **145** 628
[58] Cardona M, Shaklee K L and Pollak F H 1967 *Phys. Rev.* **154** 696
[59] Cricenti A, Selci S, Felici A C, Ferrari L, Gavrilovich A, Goletti C and Chiarotti G 1991 *Surf. Sci.* **251** 281
[60] Selci S, Cricenti A, Felici A C, Goletti C and Chiarotti G 1991 *Phys. Rev.* B **44** 8327
[61] Pan C A and Ma T P 1980 *Appl. Phys. Lett.* **37** 163
[62] Bertness K A, Kendelewicz T, List R S, Williams M D, Lindau I and Spicer W E 1986 *J. Vac. Sci. Technol.* A **4** 1424
[63] Hollinger G, Bergignat E, Joseph J and Robach Y 1985 *J. Vac. Sci. Technol.* A **3** 2082
[64] Hughes G and Ludeke R 1986 *J. Vac. Sci. Technol.* B **4** 1109
[65] Wager J F, Wilmsen C W and Kazmerski L L 1983 *Appl. Phys. Lett.* **42** 589
[66] Kowalski B J, Cricenti A, Selci S, Generosi R, Orlowski B A and Chiarotti G 1993 *Phys. Rev.* B **47** 16663
[67] Cricenti A and Felici A C 1995 *Surf. Sci.* **331** 1172
[68] Cricenti A and Felici A C 1995 *J. Vac. Sci. Technol.* A **13** 1913
[69] Kowalski B J, Cricenti A and Orlowski B A 1995 *Surf. Sci.* **338** 183
[70] Magnusson K O, Flodstrom S A and Persson P E S 1988 *Phys. Rev.* B **38** 5384
[71] Magnusson K O, Reihl B and Persson P E S 1990 *Surf. Sci.* **233** L233
[72] Cricenti A, Selci S, Magnusson K O and Reihl B 1990 *Phys. Rev.* B **41** 12908
[73] Silberman J A, Laser D, Lindau I, Spicer W E and Wilson J A 1985 *J. Vac. Sci. Technol.* A **3** 222
[74] Langmuir J 1918 *Am. Chem. Soc.* **40** 1361